Version of Record: https://www.sciencedirect.com/science/article/pii/S0142061519338967
Manuscript_ee90e036bf307ec312632b7b6892965d

Continuous-Time Look-Ahead Flexible Ramp Scheduling in Real-time Operation

A. Bagherinezhad[a], R. Khatami[a], M. Parvania[a,*]

[a]*Department of Electrical and Computer Engineering, University of Utah*

Abstract

This paper develops a novel continuous-time look-ahead optimization model for co-optimizing balancing energy and flexible ramp products in real-time power systems operation. In addition, a continuous-time day-ahead operation model is developed to commit and schedule an adequate subset of generating units for providing balancing energy and ramping requirements in real-time operation. The up and down flexible ramp products are defined as continuous-time decision trajectories that continuously supply the real-time up and down ramping requirements of the system. The deliverability of flexible ramp products is secured through reserving the respective power requirements in generation capacity constraints of generating units. A function space solution method is proposed to reduce the dimensionality of day-ahead and real-time models through projecting them into finite-dimensional function spaces spanned by Bernstein polynomials, where the real-time operation decisions are modeled with a higher accuracy level than day-ahead decisions. Simulations are conducted on the IEEE-RTS system using CAISO load data, and the numerical results showcase the effectiveness of the proposed model in supplying the energy and flexible ramp requirements and avoiding ramping scarcity in the system, while reducing the operation costs.

Keywords: Continuous-time optimization, look-ahead operation, flexible ramp product

*Corresponding author

Email addresses: avi.bagherinezhadsowmesaraee@utah.edu (A. Bagherinezhad), roohallah.khatami@utah.edu (R. Khatami), masood.parvania@utah.edu (M. Parvania)

1. Introduction

1.1. Problem Description and Background

Renewable energy integration in power systems has gained considerable momentum over the past decade and is expected to continue growing faster in near future. According to the International Energy Agency (IEA) [1], an increase of 43% is expected in global renewable electricity at year 2022 compared to 2017, forming 30% of the electricity portfolio at the time. In United States, the California's Renewable Portfolio Standard (RPS) and the New York's Renewable Energy Vision (REV) require public utilities procure at least 50% of their supplied electricity from renewable energy resources by 2030 [2, 3]. This paradigm shift in energy protfolio faces the power system operators with new challenges for supplying the increasing real-time ramp requirements and net-load imbalances [4, 5, 6].

In order to address these challenges, multiple independent system operators (ISOs), including California ISO (CAISO) and Midcontinent ISO (MISO), have introduced flexible ramp products in their day-ahead and real-time markets, which schedules additional capacity to provide extra ramping margins and prevent ramping scarcity events in real-time operation. Models are developed in [7, 8, 9, 10, 11] to schedule flexible ramp products requirement from thermal generating units, demand response and distributed energy resources in day-ahead operation. The fast ramping capability of battery energy storage and aggregate ramping capability of microgrids are deployed in [10, 11] to provide flexible ramp requirements as well as energy and reserve in day-ahead markets. Flexible ramp products are also procured in real-time markets [12, 13]. The authors in [14] investigate the impacts of flexible ramp products on real-time market by comparing deterministic and stochastic models in 5-minute dispatch and further probe into the same problem considering unit commitment in 15 minutes intervals [15]. The ramping capability of electric vehicles is deployed in [16] to help low ramp generating units to cater the real-time ramp requirements of power systems.

The flexible ramp scheduling models proposed in technical literature do not define ramping as an explicit variable, and simply define ramping as finite difference of discrete power schedules of resources. In addition, while the flexible ramp product is provided in small sub-hourly intervals, it is scheduled by coarse discrete-time optimization models with decision intervals that are larger than binding interval of the ramping products. Therefore, the current discrete-time models for scheduling flexible ramp products do not appropri-

ately model the ramping of resources that may result in schedules that are not deliverable and are in conflict with the energy and reserve schedules of generating units.

As an alternative modeling approach, continuous-time optimization methods provide an accurate model for ramping of generating units, where ramping is defined as an explicit decision variable that is equal to time derivative of continuous-time power trajectory of generating units [17, 18]. Our previous works in [17, 18, 19] have demonstrated the proficiency of continuous-time models to more efficiently deploy the flexibility of generating units in day-ahead markets. The current continuous-time operation models, however, have focused on energy markets and have not explored the application in scheduling flexible ramp products.

1.2. Contribution and Paper Structure

This paper proposes a novel continuous-time look-ahead optimization model to co-optimize energy and flexible ramp products in real-time power systems operation. The look-ahead optimization model is formulated and solved over receding horizons, where the first instant of control decisions is implemented at each run and the rest are provided as advisory schedules. The proposed model receives the real-time deviations of electricity load and solar generation, as well as the up and down flexible ramp requirements as input parameters. The outputs of the proposed model are real-time generation dispatch and the optimal flexible ramp schedule for generating units. This paper models the up and down flexible ramp capacity provided by generating units as explicit continuous-time decision variables and ensures the deliverability of ramping capacity by reserving the respective energy requirement in generation capacity constraints of units. In addition, regulation up and down capacity of generating units are modeled by continuous-time trajectories and their respective ramping requirement is accounted for in the ramping constraints of units.

The proposed real-time operation model relies on optimal schedules of generating units received from the day-ahead operation. In order to ensure the availability of adequate energy and ramping capacity for real-time operation, an enhanced continuous-time day-ahead unit commitment (UC) model is also developed to co-optimize the energy as well as balancing and regulation reserve over day-ahead scheduling horizon. The up and down balancing reserve capacities are defined and scheduled in the proposed day-ahead model to reserve capacity for supplying the real-time net-load deviation.

A function space solution method is also developed to solve the proposed continuous-time problems. The proposed solution method reduces the dimensionality of continuous-time trajectories by projecting them on a finite-dimensional function space spanned by Bernstein polynomials. The proposed solution method enables modeling differentiation and integration operations in the problems using algebraic equations in Bernstein function space. In addition, the convex hull property of Bernstein polynomials is utilized to model the continuous-time inequality constraints using finite number of constraints on the Bernstein coefficients. As the real-time operation problem requires solution in finer time resolution than the day-ahead problem, the proposed solution method utilizes function space with higher accuracy to model trajectories in the real-time operation. The proposed solution method converts the continuous-time real-time and day-ahead operation problems respectively into linear programming (LP) and mixed-integer linear programming (MILP) problems, which can be solved using commercial solvers.

The rest of the paper is organized as follows: An overview of the proposed models is presented in Section 2. The formulation of the proposed continuous-time day-ahead scheduling model as well as the look-ahead real-time energy and flexible ramp scheduling model is presented in Section 3. The proposed function space solution method to convert the continuous-time problems into LP and MILP problems is presented in Section 4. The numerical results of implementing the proposed models on the IEEE Reliability Test System (RTS) are presented in Section 5 and the conclusions are drawn in Section 6.

1.3. Notation

The following notation is used throughout the paper: boldface letters indicate the matrices and vectors. The superscripts d, u, DA, RT and $*$ represent the indices of down, up, day-ahead, real-time and optimal values and the subscripts e represent the energy. The letters G, R, B, F and I respectively represent the generation schedule, regulation, balancing reserve, flexible ramp and commitment status of the generating units. The dots over decision variables, i.e., $\dot{G}$ and $\dot{I}$ represent their time-derivatives. The overlined/underlined letters represent upper/lower limits of the trajectories. The continuous-time is t, specific time periods in day-ahead are presented by $\mathcal{T}_n = [t_n, t_{n+1}]$, and real-time receding horizons are shown by $\mathcal{T}_\tau = [\tau, \tau + T]$.

2. Overview of the Proposed Model

This section presents an overview of the proposed model for continuous-time day-ahead and real-time operations of power systems with flexible ramp products, balancing reserve, and regulation reserve. The structure of the proposed models including pertinent inputs and outputs is shown in Fig. 1.

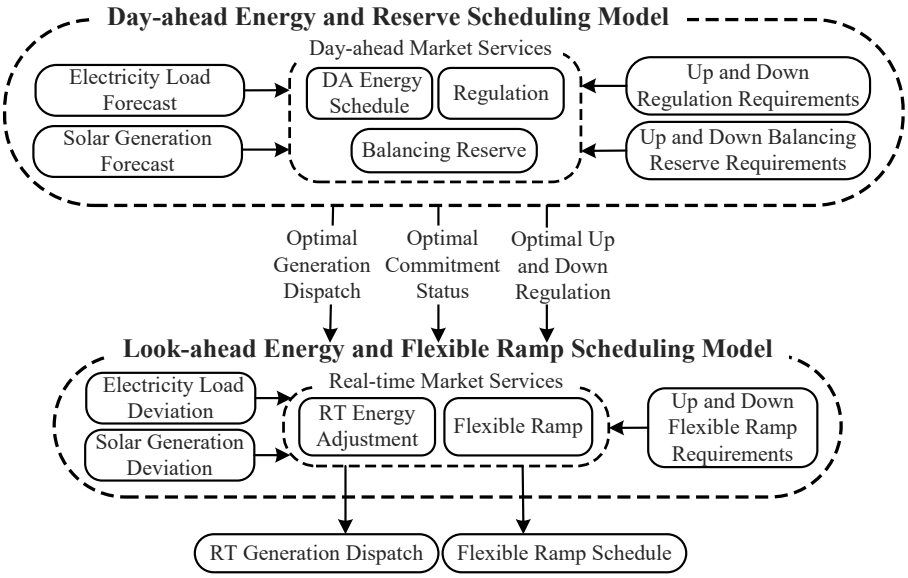

Figure 1: Structure of the proposed day-ahead and real-time look-ahead operation models

An enhanced continuous-time day-ahead unit commitment (UC) model is first developed that co-optimizes the energy, balancing reserve, and regulation reserve over the scheduling horizon $\mathcal{T}$. The up and down balancing reserve capacities are defined and scheduled in the proposed day-ahead model to reserve capacity for spplying the net-load deviation from day-ahead net-load forecast in real-time operation [20], while regulation reserve is provided by the automatic generation control (AGC) of units for load balancing in a finer temporal resolution. As shown in Fig. 1, the proposed day-ahead operation model receives the electricity load forecast, solar generation forecast, and up/down regulation and balancing reserve requirements as input parameters while the optimal commitment statuses and generation dispatch of units, as well as the associated scheduled regulation capacity, form the outputs and are used by the proposed look-ahead real-time operation model.

A continuous-time look-ahead real-time operation model is then proposed to co-optimize energy adjustments and flexible ramp products in real-time operation. The real-time look-ahead optimization model is formulated and solved over receding horizons $\mathcal{T}_\tau = [\tau, \tau{+}T]$, as schematically shown in Fig. 2, where the first instant of control decisions is implemented at each run and the rest are provided as advisory schedules. In Fig. 1, in addition to the optimal schedules received from the day-ahead model, the proposed real-time model also receives the real-time deviations of electricity load and solar generation, as well as the up and down flexible ramp requirements as input parameters. The outputs of the proposed model are real-time generation dispatch and the optimal flexible ramp schedule for generating units.

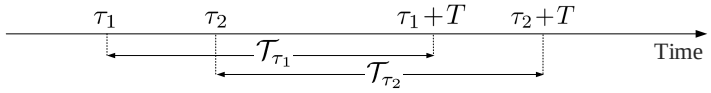

Figure 2: Real-time receding horizons in the proposed look-ahead optimization model

The proposed day-ahead and real-time scheduling models ensure allocating adequate amounts of power and ramping capacity to different services in the markets. The power and ramping capacity allocated to different services for a hypothetical generating unit is illustrated in Figs. 3. The solid black lines specify the day-ahead generation and ramping of the unit and the dotted and dashed lines represent respectively the minimum and maximum available power and ramping capacity of the unit. The areas between the lines represent the capacities allocated to the day-ahead and real-time services.

3. Proposed Continuous-time Day-ahaed and Real-time Optimization Models

3.1. Continuous-time Day-ahead Operation Model

The proposed continuous-time day-ahead operation model is formulated in (1)-(16), which co-optimizes the energy, regulation and balancing reserves provided by a set of K generating units, in order to economically supply the day-ahead net-load $N^{DA}(t)$, and cater for reserve requirements of the system. The generating units are modeled by continuous-time generation trajectories, $\mathbf{G}^{DA}(t)$, binary commitment variables, $\mathbf{I}(t)$, and ramping trajectories,

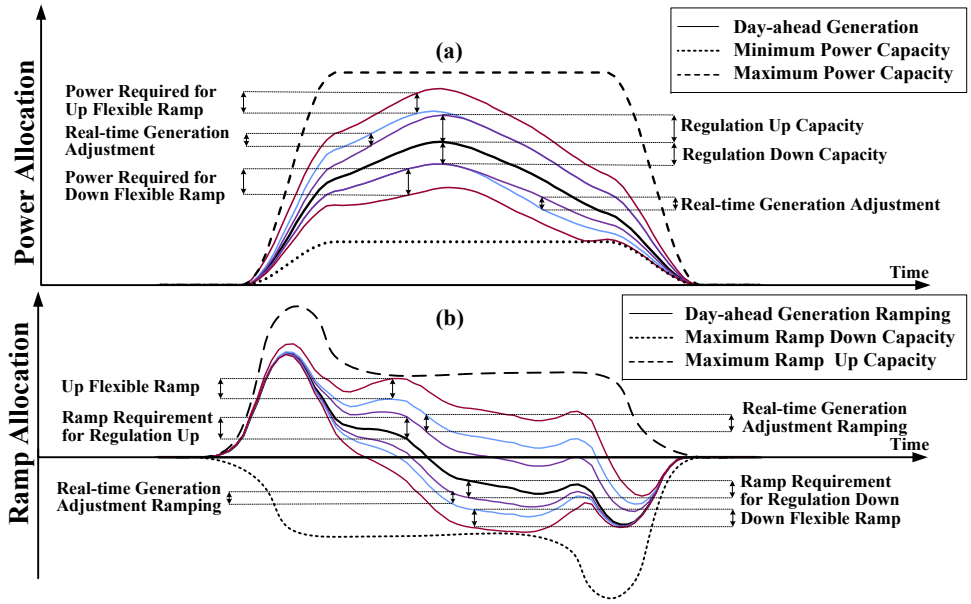

Figure 3: a) Power capacity and b) ramping capacity allocation of a generating unit

$\dot{\mathbf{G}}^{DA}(t)$, that are defined as time-derivative of the respective generation trajectories. The continuous-time trajectories of the up and down regulation and balancing reserves are respectively modeled by positive variable vectors $\mathbf{R}^u(t)$, $\mathbf{R}^d(t)$, $\mathbf{B}^u(t)$ and $\mathbf{B}^d(t)$, while the positive vectors $\mathbf{SU}(t)$ and $\mathbf{SD}(t)$ represent the startup and shutdown cost variables. The proposed day-ahead model aims at minimizing the objective functional (1) over the scheduling horizon $\mathcal{T}$ subject to the continuous-time operation constraints (2)-(16):

$$\begin{aligned}\min \int_{\mathcal{T}} \Big(& C\big(\mathbf{G}^{DA}(t)\big) + \mathbf{1}_K^T\big(\mathbf{SU}(t) + \mathbf{SD}(t)\big) \\ & + \boldsymbol{\mu}^{u,R}\mathbf{R}^u(t) + \boldsymbol{\mu}^{d,R}\mathbf{R}^d(t) \\ & + \boldsymbol{\mu}^{u,B}\mathbf{B}^u(t) + \boldsymbol{\mu}^{d,B}\mathbf{B}^d(t)\Big)\, dt, \qquad (1)\end{aligned}$$

$$\text{s.t.} \quad \mathbf{1}_K^T\mathbf{G}^{DA}(t) = N^{DA}(t), \qquad (2)$$

$$\mathbf{1}_K^T\mathbf{R}^u(t) \geq R^{u,req}(t), \qquad (3)$$

$$\mathbf{1}_K^T\mathbf{R}^d(t) \geq R^{d,req}(t), \qquad (4)$$

$$\mathbf{1}_K^T\mathbf{B}^u(t) \geq B^{u,req}(t), \qquad (5)$$

$$\mathbf{1}_K^T\mathbf{B}^d(t) \geq B^{d,req}(t), \qquad (6)$$

$$\mathbf{G}^{DA}(t) - \mathbf{R}^{d}(t) - \mathbf{B}^{d}(t) \geq \underline{\mathbf{G}}\mathbf{I}(t), \tag{7}$$

$$\mathbf{G}^{DA}(t) + \mathbf{R}^{u}(t) + \mathbf{B}^{u}(t) \leq \overline{\mathbf{G}}\mathbf{I}(t), \tag{8}$$

$$\dot{\mathbf{G}}^{DA}(t) - \frac{\mathbf{R}^{d}(t)}{T_R} - \mathbf{B}^{d}(t) \geq \underline{\dot{\mathbf{G}}}\mathbf{I}(t) + \overline{\dot{\mathbf{G}}}^{SD} \int_{t-\epsilon}^{t+\epsilon} \dot{\mathbf{I}}(t')dt', \tag{9}$$

$$\dot{\mathbf{G}}^{DA}(t) + \frac{\mathbf{R}^{u}(t)}{T_R} + \mathbf{B}^{u}(t) \leq \overline{\dot{\mathbf{G}}}\mathbf{I}(t) + \overline{\dot{\mathbf{G}}}^{SU} \int_{t-\epsilon}^{t+\epsilon} \dot{\mathbf{I}}(t')dt', \tag{10}$$

$$-\frac{\mathbf{R}^{d}(t)}{T_R} - \mathbf{B}^{d}(t) \geq \underline{\dot{\mathbf{G}}}\mathbf{I}(t), \tag{11}$$

$$\frac{\mathbf{R}^{u}(t)}{T_R} + \mathbf{B}^{u}(t) \leq \overline{\dot{\mathbf{G}}}\mathbf{I}(t), \tag{12}$$

$$\mathbf{SU}(t) \geq \mathbf{V} \int_{t-\epsilon}^{t+\epsilon} \dot{\mathbf{I}}(t')dt', \quad \mathbf{SU}(t) \geq \mathbf{0}, \tag{13}$$

$$\mathbf{SD}(t) \geq \mathbf{W} \int_{t-\epsilon}^{t+\epsilon} -\dot{\mathbf{I}}(t')dt', \quad \mathbf{SD}(t) \geq \mathbf{0}, \tag{14}$$

$$\int_{t}^{t+\mathbf{UT}} \mathbf{I}(t')dt' \geq \mathrm{Diag}(\mathbf{UT}) \int_{t-\epsilon}^{t+\epsilon} \dot{\mathbf{I}}(t')dt', \tag{15}$$

$$\int_{t}^{t+\mathbf{DT}} (\mathbf{1} - \mathbf{I}(t'))dt' \geq \mathrm{Diag}(\mathbf{DT}) \int_{t-\epsilon}^{t+\epsilon} -\dot{\mathbf{I}}(t')dt'. \tag{16}$$

The first line in (1) includes the total generation costs of units $C^{G}\big(\mathbf{G}^{DA}(t)\big)$, plus total startup and shutdown costs, where $\mathbf{1}_K$ is a K-dimensional vector of ones. The second and third lines in (1) include the costs of up and down regulation and balancing reserves provided by units, where $\boldsymbol{\mu}^{u,R}$, $\boldsymbol{\mu}^{d,R}$, $\boldsymbol{\mu}^{u,B}$, $\boldsymbol{\mu}^{d,B}$ are row vectors of the associated cost coefficients. The continuous-time supply of day-ahead net-load is ensured in (2), while the up and down regulation and balancing reserve requirements of the system are met in (3)-(6). The power capacity and ramping capability limits of generating units are imposed in (7)-(12). In (7), the scheduled generation minus regulation down and balancing reserve down capacity is limited to the minimum generation limits of units, while the summation of scheduled generation, regulation up and balancing reserve up capacities is confined in (8) to the maximum generation limits. The diagonal matrices $\underline{\mathbf{G}}$ and $\overline{\mathbf{G}}$ in (7) and (8) repectively represent the minimum and maximum limits of units. The continuous-time ramping trajectories of generating units, adjusted with ramp requirements of regulation and balancing reserve, are constrained in (9) and (10) where

$\underline{\dot{\mathbf{G}}}$, $\overline{\dot{\mathbf{G}}}$, $\overline{\dot{\mathbf{G}}}^{SU}$ and $\overline{\dot{\mathbf{G}}}^{SD}$ are diagonal matrices representing respectively the minimum and maximum ramping of units, and the associated start-up and shutdown ramping limits. The second terms in left-hand-side of (9) and (10) ensure that there is enough ramping capability to fully deploy the reserved regulation up and down capacity, where T_R is the regulation binding horizon (e.g., 5 minutes in CAISO [21]). The adequacy of generating units ramping capability for supplying regulation and balancing reserve is secured in (11) and (12). The start up and shut down costs, $\mathbf{SU}(t)$ and $\mathbf{SD}(t)$, are calculated in (13) and (14), where $\mathbf{V}$ and $\mathbf{W}$ represent diagonal matrices of start up and shut down costs of units. The minimum up and down time constraints of units are imposed through (15) and (16), in which $\mathbf{UT}$ and $\mathbf{DT}$ are respectively vectors of minimum up and down times of generating units. In (9)-(10) and (13)-(16), $\dot{\mathbf{I}}(t)$ is the time derivative of commitment variables that indicates the start up and shut down of generating units and ϵ is a very small positive number.

3.2. Continuous-time Look-ahead Real-time Operation Model

The proposed continuous-time look-ahead real-time operation model optimally adjusts the day-ahead schedule of units in order to match the real-time net-load forecast and real-time up/down flexible ramp requirements, where the optimal day-ahead decision trajectories are deemed as input parameters and denoted with asterisks. The deviation of real-time net-load, $N^{RT}(t)$, from day-ahead net-load is represented by $n(t) = N^{RT}(t) - N^{DA}(t)$. In the proposed model, generating units continuously adjust their day-ahead generation schedule to counterbalance $n(t)$ where their up real-time generation adjustment trajectories, $\mathbf{G}^{RT,u}(t)$, balance the positive net-load deviations, and down real-time generation adjustment trajectories, $\mathbf{G}^{RT,d}(t)$, balance the negative deviations and up and down real-time generation ramping trajectories are represented by $\dot{\mathbf{G}}^{RT,u}(t)$ and $\dot{\mathbf{G}}^{RT,d}(t)$, respectively. The continuous-time up and down flexible ramp product trajectories of generating units are shown by vectors $\mathbf{F}^u(t)$ and $\mathbf{F}^d(t)$, which reserve additional ramping capacity to supply the net-load uncertainties in real-time operation. The proposed continuous-time look-ahead real-time operation model is formulated as a variational optimization problem, which minimizes the objective functional (17) subject to the continuous-time equality and inequality constraints (18)-(24)

as below:

$$\begin{aligned}
\min J = \int_{\mathcal{T}_\tau} \big(& \boldsymbol{\mu}^{u,G}\mathbf{G}^{RT,u}(t) + \boldsymbol{\mu}^{d,G}\mathbf{G}^{RT,d}(t) \\
& + \boldsymbol{\mu}^{u,F}\mathbf{F}^{u}(t) + \boldsymbol{\mu}^{d,F}\mathbf{F}^{d}(t) \\
& + \mu^{u,S_e} S_e^u(t) + \mu^{d,S_e} S_e^d(t) \\
& + \mu^{u,S_F} S_F^u(t) + \mu^{d,S_F} S_F^d(t) \big) dt, \qquad (17)
\end{aligned}$$

$$\text{s.t.} \quad n(t) = \mathbf{1}_K^T(\mathbf{G}^{RT,u}(t) - \mathbf{G}^{RT,d}(t)) - S_e^u(t) + S_e^d(t), \qquad t \in \mathcal{T}_\tau, \qquad (18)$$

$$\mathbf{1}_K^T \mathbf{F}^u(t) \geq FRR^u(t) - S_F^u(t), \qquad t \in \mathcal{T}_\tau, \qquad (19)$$

$$\mathbf{1}_K^T \mathbf{F}^d(t) \geq FRR^d(t) - S_F^d(t), \qquad t \in \mathcal{T}_\tau, \qquad (20)$$

$$\mathbf{G}^{DA^*}(t) - \mathbf{R}^{d^*}(t) - \mathbf{G}^{RT,d}(t) - \int_t^{t+T_F} \mathbf{F}^d(t')dt' \geq \underline{\mathbf{G}}(t), \ t \in \mathcal{T}_\tau, \qquad (21)$$

$$\mathbf{G}^{DA^*}(t) + \mathbf{R}^{u^*}(t) + \mathbf{G}^{RT,u}(t) + \int_t^{t+T_F} \mathbf{F}^u(t')dt' \leq \overline{\mathbf{G}}(t), \ t \in \mathcal{T}_\tau, \qquad (22)$$

$$\dot{\mathbf{G}}^{DA^*}(t) - \frac{\mathbf{R}^{d^*}(t)}{T_R} + \dot{\mathbf{G}}^{RT,u}(t) - \dot{\mathbf{G}}^{RT,d}(t) - \mathbf{F}^d(t) \geq \underline{\dot{\mathbf{G}}}(t), \ t \in \mathcal{T}_\tau, \qquad (23)$$

$$\dot{\mathbf{G}}^{DA^*}(t) + \frac{\mathbf{R}^{u^*}(t)}{T_R} + \dot{\mathbf{G}}^{RT,u}(t) - \dot{\mathbf{G}}^{RT,d}(t) + \mathbf{F}^u(t) \leq \overline{\dot{\mathbf{G}}}(t), \ t \in \mathcal{T}_\tau, \qquad (24)$$

$$-\frac{\mathbf{R}^{d^*}(t)}{T_R} - \mathbf{F}^d(t) \geq \underline{\dot{\mathbf{G}}}(t), \qquad t \in \mathcal{T}_\tau, \qquad (25)$$

$$\frac{\mathbf{R}^{u^*}(t)}{T_R} + \mathbf{F}^u(t) \leq \overline{\dot{\mathbf{G}}}(t), \qquad t \in \mathcal{T}_\tau. \qquad (26)$$

The objective functional (17) minimizes the total real-time operation cost of the system over the look-ahead scheduling horizon $\mathcal{T}_\tau$, which includes in the first and second lines the cost of real-time generation adjustment and flexible ramp procurement by generating units, respectively. The terms $\boldsymbol{\mu}^{u,G}$, $\boldsymbol{\mu}^{d,G}$, $\boldsymbol{\mu}^{u,F}$, $\boldsymbol{\mu}^{d,F}$ are respectively cost vectors of up and down generation adjustment and flexible ramp capacity of generating units, and $\mathbf{1}_K$ is a K-dimensional vector of ones. The third and fourth lines in (17) represent the cost of not supplying the real-time net-load deviation and flexible ramp products due to energy and ramping capacity scarcity, where $S_e^u(t)$, $S_e^d(t)$, $S_F^u(t)$ and $S_F^d(t)$ are variables respectively representing real-time up and down energy and flexible ramp scarcity trajectories. The price of up and down energy and flexible ramp scarcity are respectively denoted by μ^{u,S_e}, μ^{d,S_e}, μ^{u,S_F}, μ^{d,S_F}.

The continuous-time real-time power balance constraint (18) ensures that the up and down real-time adjustment trajectories of generating units supply the real-time net-load deviation from the day-ahead net-load, except some scarcity events that are measured by $S_e^u(t)$ and $S_e^d(t)$. The procurement of up and down flexible ramp requirements, $FRR^u(t)$ and $FRR^d(t)$, is secured in (19) and (20) except for flexible ramp scarcity events where the amount of up and down scarcity are measured by $S_F^u(t)$ and $S_F^d(t)$. The adequacy of generation and ramping capacity of generating units to accommodate the required energy, regulation and flexible ramp is ensured in (21)-(24). In (21), the optimal day-ahead generation minus the optimal day-ahead reserved regulation down capacity, the downward real-time generation adjustment, and the generation capacity reserved for delivering flexible ramp down is limited to the minimum generation limit of units, $\underline{\mathbf{G}}(t)$. In (22), the optimal day-ahead generation plus the optimal reserved regulation up capacity, the upward real-time generation adjustment and the generation capacity reserved for delivering flexible ramp up is limited to the maximum generation limit of units, $\overline{\mathbf{G}}(t)$. The integrals in (21) and (22) calculate the required energy for delivering the flexible ramp capacity in the binding horizon T_F (e.g., 5 minutes in CAISO [22]), in which the initial values are considered zero (i.e., $\mathbf{F}^d(\tau)=\mathbf{0}, \mathbf{F}^u(\tau)=\mathbf{0}$). The down and up ramping constraints of generating units are formulated in (23) and (24). In (23), optimal day-ahead generation ramping, $\dot{\mathbf{G}}^{DA^*}(t)$, minus the required ramp to provide the reserved day-ahead regulation down capacity plus the net real-time generation ramping minus down flexible ramp is limited to the units ramping down capability, $\underline{\dot{\mathbf{G}}}(t)$. Further, in (24), the day-ahead generation ramping plus the required ramp to supply the reserved day-ahead regulation up capacity plus the net real-time generation ramping plus up flexible ramp is limited to the units ramping up capability, $\overline{\dot{\mathbf{G}}}(t)$. The adequacy of down and up ramping of generating units in the binding horizon is ensured in (25) and (26).

3.3. Estimating Flexible Ramp Requirements

Let the real-time net-load error at time t, represented by $\epsilon(t)$, follow a Gaussian distribution with mean $m_\epsilon(t)$ and standard deviation $\sigma_\epsilon(t)$, i.e., $\epsilon(t) \sim \mathcal{N}(m_\epsilon(t), \sigma_\epsilon(t))$, where the probability distribution function of the real-time net-load forecast error is shown by $P_e(\epsilon(t))$. The upper and lower confidence levels of the flexible ramp uncertainty, UCL and LCL, are dictated by the system operator (e.g., $LCL = 0.05$ and $UCL = 0.95$), which leads to

calculating the uncertainty at upper and lower confidence levels, $\alpha^u(t)$ and $\alpha^d(t)$, respectively from (27) and (28):

$$UCL = \int_{-\infty}^{\alpha^u(t)} P_e(\epsilon(t))d\epsilon(t), \tag{27}$$

$$LCL = \int_{-\infty}^{\alpha^d(t)} P_e(\epsilon(t))d\epsilon(t). \tag{28}$$

The values of $\alpha^u(t)$ and $\alpha^d(t)$ from (27) and (28) are respectively substituted in (29) and (30) to calculate the forecast error uncertainty of the up and down flexible ramp at upper and lower confidence levels, $U^u(t)$ and $U^d(t)$, as follows:

$$U^u(t) = \max(0, \alpha^u(t)), \qquad t \in \mathcal{T}_\tau, \tag{29}$$

$$U^d(t) = \min(0, \alpha^d(t)), \qquad t \in \mathcal{T}_\tau. \tag{30}$$

The up and down flexible ramp requirements in real-time operation are functions of the forecast error uncertainty and ramping of the real-time net-load, defined as below:

$$FRR^d(t) = -\min(0, U^d(t) + \max(0, \dot{n}(t))), \quad t \in \mathcal{T}_\tau, \tag{31}$$

$$FRR^u(t) = \max(0, U^u(t) + \min(0, \dot{n}(t))), \qquad t \in \mathcal{T}_\tau. \tag{32}$$

In (31), flexible ramp down requirement trajectory at time t is the minimum of zero and the sum of forecast error uncertainty of flexible ramp at lower confidence level and the positive part of real-time net-load ramping, multiplied by -1. Further, flexible ramp up requirement trajectory in (32) is equal to maximum of zero and the sum of forecast error uncertainty of flexible ramp at upper confidence level and the negative part of real-time net-load ramping.

4. The Proposed Computational Solution

The decision space of the proposed continuous-time optimization models in (1)-(16) and (17)-(24) are infinite dimensional, which makes the solution of the models computationally intractable. In this regard, we expand on our previous works in [17, 18] and develop a function space solution method for solving the proposed continuous-time day-ahead and real-time scheduling problems.

The proposed method utilizes Bernstein polynomials of degree Q for modeling the continuous-time trajectories, which are defined as [23]:

$$b_{q,Q}(t) = \binom{Q}{q} t^q (1-t)^{Q-q}, \quad t \in [0,1), q = 0, ..., Q. \tag{33}$$

The proposed solution method involves modeling the continuous-time day-ahead and real-time trajectories with different levels of accuracy as required to match the variability of net-load in day-ahead and real-time operations.

In day-ahead operation model, the scheduling horizon is divided to a set of intervals (e.g., hourly) within which the continuous-time trajectories are modeled with Bernstein splines of degree Q, while C^1 continuity conditions are imposed at the connection points between intervals to maintain the smoothness of trajectories [17, 18].

In real-time operation model, however, each continuous-time trajectory spanned over the receding horizon $\mathcal{T}_\tau$ of length T (e.g., 15 minutes) is modeled with a single Bernstein polynomials of degree Q. Since the length of real-time receding horizons is shorter than the length of day-ahead model intervals, the real-time trajectories are modeled with a higher accuracy as compared to day-ahead trajectories. This is schematically illustrated in Fig. 4 where the continuous-time trajectory is denoted with the solid black curve, the Bernstein coefficients of the day-ahead and real-time trajectories are shown respectively with gray and black dots, and the associated control polygons are shown with gray and black dotted lines. As shown in Fig. 4, the control

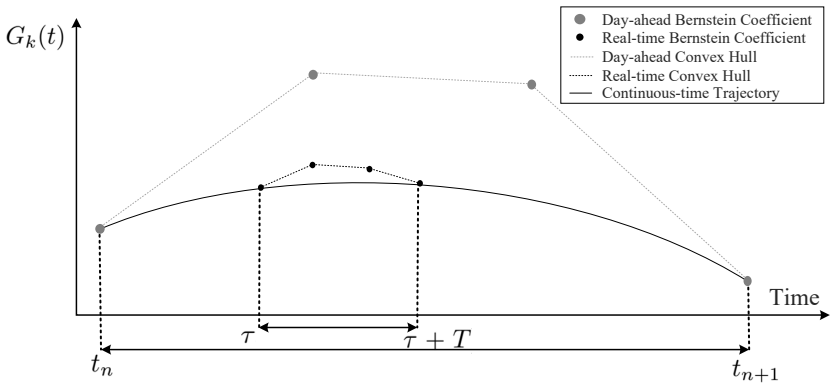

Figure 4: Coefficients of Bernstein polynomials in day-ahead and real-time models

polygon constructed by real-time Bernstein coefficients is inside the day-ahead polygon which implies adopting higher accuracy in modeling the real-time trajectories.

The function space method proposed in this paper converts the continuous-time day-ahead and real-time operation problems in (1)-(16) and (17)-(24) respectively into MILP and LP problems with Bernstein coordinates of the trajectories as decision variables. The proposed solution approach for the day-ahead and real-time models is summarized in Fig. 4, and is presented in detail in the following Subsections 4.1 and 4.2.

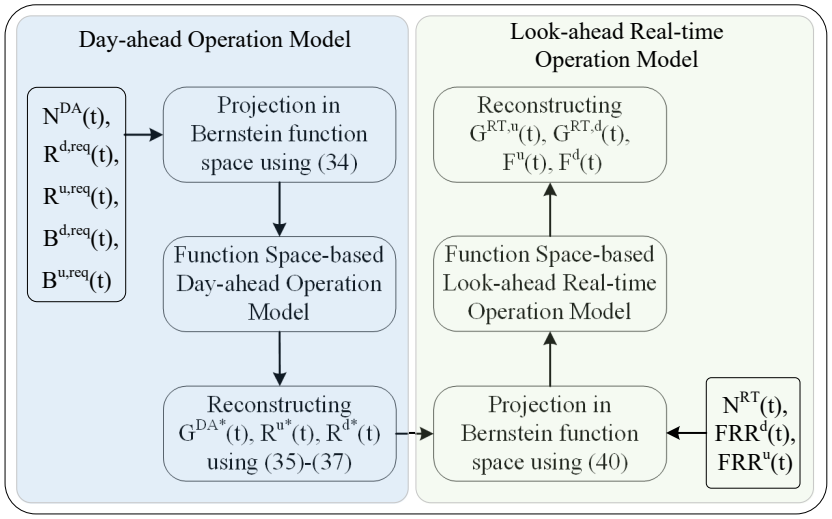

Figure 5: The proposed function space-based solution approach

4.1. Function Space Representation of the Day-ahead Scheduling Problem

In day-ahead model, we first subdivide the scheduling horizon $\mathcal{T}$ into N intervals $\mathcal{T}_n$ and then construct a subset of basis functions formed by the Bernstein polynomials of degree Q in each interval $\mathcal{T}_n$, which leads to forming a spline function space to represent the whole scheduling horizon $\mathcal{T}$. Thus, the vector of basis functions $\mathbf{e1}^{(Q)}(t) = (e1_1^{(Q)}(t), \ldots, e1_P^{(Q)}(t))^T$ spanning $\mathcal{T}$ contains $P = (Q+1)N$ functions with components defined as:

$$e1^{(Q)}_{n(Q+1)+q}(t) = b_{q,Q}\left(\frac{t-t_n}{T_n}\right), t \in [t_n, t_{n+1}), \tag{34}$$

for $n = 0, \ldots, N-1; q = 0, \ldots, Q$. To reduce notation, we define $p \equiv n(Q+1)+q$, where p goes from 0 to $(Q+1)N-1$.

The continuous-time generation of the generating units, as well as the associated up and down regulation and balancing reserve, are modeled in the space spanned by $\mathbf{e1}^{(Q)}(t)$ as follows:

$$\mathbf{G}^{DA}(t) = \mathbf{G}^{DA}\mathbf{e1}^{(Q)}(t), \tag{35}$$

$$\mathbf{R}^{u}(t) = \mathbf{R}^{u}\mathbf{e1}^{(Q)}(t), \tag{36}$$

$$\mathbf{R}^{d}(t) = \mathbf{R}^{d}\mathbf{e1}^{(Q)}(t), \tag{37}$$

$$\mathbf{B}^{u}(t) = \mathbf{B}^{u}\mathbf{e1}^{(Q)}(t), \tag{38}$$

$$\mathbf{B}^{d}(t) = \mathbf{B}^{d}\mathbf{e1}^{(Q)}(t), \tag{39}$$

where $\mathbf{G}^{DA}$, $\mathbf{R}^{u}$, $\mathbf{R}^{d}$, $\mathbf{B}^{u}$ and $\mathbf{B}^{d}$ are $K \times P$ matrices of Bernstein coefficients. The rereads are referred to [18, 24, 25] for a detailed account of day-ahead model representation in Bernstein function space.

4.2. Function Space Representation of the Real-time Scheduling Problem

In real-time continuous-time flexible ramp scheduling model, the splines are formed in one interval over look-ahead scheduling horizon $\mathcal{T}_\tau$ of length T, in which the vector of basis function $\mathbf{e2}^{(Q)}(t) = \left(e2_1^{(Q)}(t), \ldots, e2_{(Q+1)}^{(Q)}(t)\right)^T$ is defined as:

$$e2_q^{(Q)}(t) = b_{q,Q}\left(\frac{t-\tau}{T}\right),\ t \in \mathcal{T}_\tau,\ q = 0, ..., Q. \tag{40}$$

Below, we model different components of continuous-time look-ahead energy and ramp scheduling problem in the real-time operation of the power system assuming $\mathbf{e2}^{(Q)}(t)$ as the basis function.

4.2.1. Modeling the Generation Adjustment Trajectories

The up and down real-time generation adjustment trajectories of the generating units are modeled in function space spanned by $\mathbf{e2}^{(Q)}(t)$ as follows:

$$\mathbf{G}^{RT,u}(t) = \mathbf{G}^{RT,u}\mathbf{e2}^{(Q)}(t), \qquad t \in \mathcal{T}_\tau, \tag{41}$$

$$\mathbf{G}^{RT,d}(t) = \mathbf{G}^{RT,d}\mathbf{e2}^{(Q)}(t), \qquad t \in \mathcal{T}_\tau, \tag{42}$$

where $\mathbf{G}^{RT,u}$ and $\mathbf{G}^{RT,d}$ are $K \times (Q+1)$ matrices of Bernstein coefficients.

4.2.2. Modeling the Real-time Generation Adjustment Ramping Trajectories

A linear combination of Bernstein polynomials can relate the Bernstein polynomials of degree Q and their time-derivatives of degree $Q-1$ [26]. This property of the Bernstein polynomials lets us define the up and down real-time generation adjustment ramping trajectories in function space spanned by Bernstein polynomials of degree $Q-1$, $\mathbf{e2}^{(Q-1)}(t)$, as follows:

$$\dot{\mathbf{G}}^{RT,u}(t)=\mathbf{G}^{RT,u}\dot{\mathbf{e2}}^{(Q)}(t)=\mathbf{G}^{RT,u}\mathcal{M}\mathbf{e2}^{(Q-1)}(t)=\dot{\mathbf{G}}^{RT,u}\mathbf{e2}^{(Q-1)}(t), \tag{43}$$

$$\dot{\mathbf{G}}^{RT,d}(t)=\mathbf{G}^{RT,d}\dot{\mathbf{e2}}^{(Q)}(t)=\mathbf{G}^{RT,d}\mathcal{M}\mathbf{e2}^{(Q-1)}(t)=\dot{\mathbf{G}}^{RT,d}\mathbf{e2}^{(Q-1)}(t), \tag{44}$$

where $\mathcal{M}$ is the $(Q+1)\times Q$ matrix relating $\dot{\mathbf{e2}}^{(Q)}(t)$ and $\mathbf{e2}^{(Q-1)}(t)$, and $\dot{\mathbf{G}}^{RT,u}$ and $\dot{\mathbf{G}}^{RT,d}$ are $K\times Q$ matrices of Bernstein coefficients, which are linearly related to the associated Bernstein coefficients of up and down real-time generation adjustment trajectories as follows:

$$\dot{\mathbf{G}}^{RT,u}=\mathbf{G}^{RT,u}\mathcal{M},\quad \dot{\mathbf{G}}^{RT,d}=\mathbf{G}^{RT,d}\mathcal{M}. \tag{45}$$

4.2.3. Modeling the Flexible Ramp Trajectories

The flexible ramp trajectories are ramping trajectories which are modeled in the function space spanned by $\mathbf{e2}^{(Q-1)}(t)$ as:

$$\mathbf{F}^{u}(t)=\mathbf{F}^{u}\mathbf{e2}^{(Q-1)}(t),\qquad t\in\mathcal{T}_{\tau}, \tag{46}$$

$$\mathbf{F}^{d}(t)=\mathbf{F}^{d}\mathbf{e2}^{(Q-1)}(t),\qquad t\in\mathcal{T}_{\tau}. \tag{47}$$

where $\mathbf{F}^{u}$ and $\mathbf{F}^{d}$ are $K\times Q$ matrices of Bernstein coefficients.

4.2.4. Modeling the Integrals of Flexible Ramp Trajectories

The integrals of the Bernstein polynomials of degree $Q-1$ are linearly related to the Bernstein polynomials of degree Q [26], suggesting that there exists a $Q\times(Q+1)$ linear mapping $\mathcal{N}$ relating the integrals of the basis functions of degree $Q-1$ to the basis functions of degree Q. Regarding this feature, the integrals of up and down flexible ramp trajectories are modeled in the Bernstein function space spanned by $\mathbf{e2}^{(Q)}(t)$ as:

$$\int_{t}^{t+T_F}\mathbf{F}^{u}(t')dt'=\mathbf{F}^{u}\int_{t}^{t+T_F}\mathbf{e2}^{(Q-1)}(t')dt'=$$
$$\mathbf{F}^{u}\mathcal{N}\big(\mathbf{e2}^{(Q)}(t+T_F)-\mathbf{e2}^{(Q)}(t)\big)=\mathbf{F}^{u}\mathcal{N}\mathcal{X}\mathbf{e2}^{(Q)}(t),\quad t\in\mathcal{T}_{\tau}, \tag{48}$$

$$\int_{t}^{t+T_F}\mathbf{F}^{d}(t')dt'=\mathbf{F}^{d}\int_{t}^{t+T_F}\mathbf{e2}^{(Q-1)}(t')dt'=$$
$$\mathbf{F}^{d}\mathcal{N}\big(\mathbf{e2}^{(Q)}(t+T_F)-\mathbf{e2}^{(Q)}(t)\big)=\mathbf{F}^{d}\mathcal{N}\mathcal{X}\mathbf{e2}^{(Q)}(t),\quad t\in\mathcal{T}_{\tau}, \tag{49}$$

where $\mathcal{X}$ is a $(Q+1)\times(Q+1)$ matrix relating $(\mathbf{e2}^{(Q)}(t+T_F)-\mathbf{e2}^{(Q)}(t))$ and $\mathbf{e2}^{(Q)}(t)$.

4.2.5. Modeling Inequality Constraints

The convex hull property of the Bernstein polynomials states that a projected continuous-time trajectory modeled in Bernstein function space would never be outside of the convex hull of its control polygon. This property lets us efficiently impose the continuous-time inequality constraints (21)-(26).

Let the optimal continuous-time day-ahead generation and regulation reserve up and down trajectories, $\mathbf{G}^{DA^*}(t)$, $\mathbf{R}^{u^*}(t)$ and $\mathbf{R}^{d^*}(t)$ in (21) and (22) be projected into the function space spanned by $\mathbf{e2}^{(Q)}(t)$ as follows:

$$\mathbf{G}^{DA^*}(t) = \mathbf{G}^{DA^*}\mathbf{e2}^{(Q)}(t), \quad t \in \mathcal{T}_\tau, \tag{50}$$

$$\mathbf{R}^{u^*}(t) = \mathbf{R}^{u^*}\mathbf{e2}^{(Q)}(t), \quad t \in \mathcal{T}_\tau, \tag{51}$$

$$\mathbf{R}^{d^*}(t) = \mathbf{R}^{d^*}\mathbf{e2}^{(Q)}(t), \quad t \in \mathcal{T}_\tau, \tag{52}$$

where $\mathbf{G}^{DA^*}$, $\mathbf{R}^{u^*}$ and $\mathbf{R}^{d^*}$ are $K \times (Q+1)$ matrices of Bernstein coefficients. Regarding the convex hull property, the inequality constraints (19)-(26) are modeled in the Bernstein function space as follows:

$$\mathbf{1}_K^T\mathbf{F}^u \geq \mathbf{FRR}^u - \mathbf{S}_F^u, \tag{53}$$

$$\mathbf{1}_K^T\mathbf{F}^d \geq \mathbf{FRR}^d - \mathbf{S}_F^d, \tag{54}$$

$$\mathbf{G}^{DA^*} - \mathbf{R}^{d^*} - \mathbf{G}^{RT,d} - \mathbf{F}^d\mathcal{N}\mathcal{X} \geq \underline{\underline{\mathbf{G}}}, \tag{55}$$

$$\mathbf{G}^{DA^*} + \mathbf{R}^{u^*} + \mathbf{G}^{RT,u} + \mathbf{F}^u\mathcal{N}\mathcal{X} \leq \overline{\overline{\mathbf{G}}}, \tag{56}$$

$$\left[\mathbf{G}^{DA^*}\mathcal{M}+\dot{\mathbf{G}}^{RT,u}-\dot{\mathbf{G}}^{RT,d}-\mathbf{F}^d\right]\mathbf{M}-\mathbf{R}^{d^*} \geq \underline{\underline{\dot{\mathbf{G}}}}\mathbf{M}, \tag{57}$$

$$\left[\mathbf{G}^{DA^*}\mathcal{M}+\dot{\mathbf{G}}^{RT,u}-\dot{\mathbf{G}}^{RT,d}+\mathbf{F}^u\right]\mathbf{M}+\mathbf{R}^{u^*} \leq \overline{\overline{\dot{\mathbf{G}}}}\mathbf{M}, \tag{58}$$

$$-\mathbf{F}^d\mathbf{M}-\mathbf{R}^{d^*} \geq \underline{\underline{\dot{\mathbf{G}}}}\mathbf{M}, \tag{59}$$

$$\mathbf{F}^u\mathbf{M}+\mathbf{R}^{u^*} \leq \overline{\overline{\dot{\mathbf{G}}}}\mathbf{M}, \tag{60}$$

where $\mathbf{FRR}^u$, $\mathbf{FRR}^d$, $\mathbf{S}_F^u$ and $\mathbf{S}_F^d$ in (53) and (54) are Q-dimensional vectors of function space coefficients associated with the up and down flexible ramp requirement and flexible ramp scarcity trajectories; $\underline{\underline{\mathbf{G}}}$ and $\overline{\overline{\mathbf{G}}}$ in (55) and (56) are $K \times (Q+1)$ matrices of Bernstein coefficients associated with the minimum and maximum generation trajectories $\underline{\mathbf{G}}(t)$ and $\overline{\mathbf{G}}(t)$; and $\underline{\underline{\dot{\mathbf{G}}}}$ and $\overline{\overline{\dot{\mathbf{G}}}}$ in (57) and (58) are $K \times Q$ matrices of Bernstein coefficients associated

with the minimum and maximum ramping trajectories $\underline{\dot{\mathbf{G}}}(t)$ and $\overline{\dot{\mathbf{G}}}(t)$. As the Bernstein coefficients of degrees Q and $Q-1$ coexist in (57)-(60), the $Q\times(Q+1)$ degree-raising matrix $\mathbf{M}$ relating $\mathbf{e2}^{(Q-1)}(t)$ to $\mathbf{e2}^{(Q)}(t)$ is introduced to unify the function space degrees.

4.2.6. Modeling the Power Balance Constraint

The real-time net-load deviation, $n(t)$, and the up and down energy scarcity trajectories are projected into the Bernstein function space spanned by $\mathbf{e2}^{(Q)}(t)$ as follows:

$$n(t) = \mathbf{n}\mathbf{e2}^{(Q)}(t), \qquad t \in \mathcal{T}_\tau, \tag{61}$$

$$S_e^u(t) = \mathbf{S}_e^u\mathbf{e2}^{(Q)}(t), \quad t \in \mathcal{T}_\tau, \tag{62}$$

$$S_e^d(t) = \mathbf{S}_e^d\mathbf{e2}^{(Q)}(t), \quad t \in \mathcal{T}_\tau, \tag{63}$$

where $\mathbf{n}$, $\mathbf{S}_e^u$ and $\mathbf{S}_e^d$ are row vectors of Bernstein coefficients. Substituting the real-time generation adjustment trajectories from (41)-(42), the net-load deviation from (61), and the energy scarcity trajectories from (62)-(63), in (18) and eliminating $\mathbf{e2}^{(Q)}(t)$ from both sides of the equality, the function space representation of the real-time power balance constraint is cast as follows:

$$\mathbf{n} = \mathbf{1}_K^T\left(\mathbf{G}^{RT,u} - \mathbf{G}^{RT,d}\right) - \mathbf{S}_e^u + \mathbf{S}_e^d. \tag{64}$$

4.2.7. Modeling the Objective Functional

Let us substitute the continuous-time trajectories in the objective functional (17) with their function space representations as follows:

$$\begin{aligned} J = \int_{\mathcal{T}_\tau} \big[&\boldsymbol{\mu}^{u,G}\mathbf{G}^{RT,u}\mathbf{e2}^{(Q)}(t) + \boldsymbol{\mu}^{d,G}\mathbf{G}^{RT,d}\mathbf{e2}^{(Q)}(t) \\ &+ \boldsymbol{\mu}^{u,F}\mathbf{F}^u\mathbf{e2}^{(Q-1)}(t) + \boldsymbol{\mu}^{d,F}\mathbf{F}^d\mathbf{e2}^{(Q-1)}(t) \\ &+ \mu^{u,S_e}\mathbf{S}_e^u\mathbf{e2}^{(Q)}(t) + \mu^{d,S_e}\mathbf{S}_e^d\mathbf{e2}^{(Q)}(t) \\ &+ \mu^{u,S_F}\mathbf{S}_F^u\mathbf{e2}^{(Q-1)}(t) + \mu^{d,S_F}\mathbf{S}_F^d\mathbf{e2}^{(Q-1)}(t)\big]\,dt \\ = \big[&\boldsymbol{\mu}^G(\mathbf{G}^{RT,u} + \mathbf{G}^{RT,d}) + \mu^{u,S_e}\mathbf{S}_e^u + \mu^{d,S_e}\mathbf{S}_e^d\big]\int_{\mathcal{T}_\tau}\mathbf{e2}^{(Q)}(t)dt \\ +\big[&\boldsymbol{\mu}^{u,F}\mathbf{F}^u + \boldsymbol{\mu}^{d,F}\mathbf{F}^d + \mu^{u,S_F}\mathbf{S}_F^u + \mu^{d,S_F}\mathbf{S}_F^d\big]\int_{\mathcal{T}_\tau}\mathbf{e2}^{(Q-1)}(t)dt. \end{aligned} \tag{65}$$

The integrals of Bernstein polynomials of degree Q over $\mathcal{T}_\tau$ are calculated as:

$$\int_{\mathcal{T}_\tau} e2_q^{(Q)}(t) = \frac{T}{Q+1},\ q = 0,\ldots,Q. \tag{66}$$

Thus, substituting the integral values from (66) in (65) we arrive at:

$$J = T\frac{\left[\boldsymbol{\mu}^{u,G}\mathbf{G}^{RT,u} + \boldsymbol{\mu}^{d,G}\mathbf{G}^{RT,d} + \mu^{u,S_e}\mathbf{S}_e^u + \mu^{d,S_e}\mathbf{S}_e^d\right]\mathbf{1}_{Q+1}}{Q+1} + T\frac{\left[\boldsymbol{\mu}^{u,F}\mathbf{F}^u + \boldsymbol{\mu}^{d,F}\mathbf{F}^d + \mu^{u,S_F}\mathbf{S}_F^u + \mu^{d,S_F}\mathbf{S}_F^d\right]\mathbf{1}_Q}{Q}. \tag{67}$$

In summary, the proposed function space solution method in Section 4 converts the continuous-time day-ahead and real-time operation models in (1)-(16) and (17)-(24) respectively to MILP and LP problems with the Bernstein coordinates of decision trajectories as decision variables.

5. Numerical results

The numerical results of implementing the proposed models on IEEE-RTS [27] are presented in this section. The day-ahead load and solar generation data of CAISO for Feb. 1, 2018 [28] are used to generate continuous-time day-ahead load and solar trajectories which are modeled in Bernstein function space of degree 3, where the CAISO load data are first scaled down to 2850MW peak load of IEEE-RTS, and next the solar data are scaled down with the exact same ratio. The continuous-time real-time load and solar generation trajectories are derived from day-ahead counterparts through imposing error terms with respective standard deviations of %1.5 and %2. Real-time look-ahead models are run every 5 minutes and the length of receding horizons is considered to be 15 minutes.

The numerical results of discrete-time day-ahead and real-time models are also calculated through projecting the models in (1)-(16) and (17)-(24) into the Bernstein function space of degree 0. These models serve as base cases and enable highlighting the benefits of proposed continuous-time models. First, the optimal day-ahead hourly schedules are calculated from discrete-time day-ahead operation model, which convey abrupt transitions between hourly intervals, and do not reflect the actual transition process followed by the power system operators. In order to be consistent with the current operation practice, the day-ahead schedules are adjusted and the transitions between hours are made in linear paths within 20-minute intervals starting 10 minutes before each hour [29]. The adjusted schedules are then fed into the real-time look-ahead discrete-time models.

The cost coefficients of day-ahead balancing and regulation reserve capacities are respectively 0.2 and 0.3 times the highest energy bid of each unit,

the real-time flexible ramp capacity cost coefficients are the same as that for the regulation, the up and down real-time generation adjustment cost coefficients are respectively 1.5 and 1.2 times the highest energy bid of each unit, and the up and down flexible ramp scarcity prices are respectively considered as \$247/MW and \$152/MW. In the objective function (17) of the real-time model we use a penalty cost of \$3000/MW to penalize the up/down energy scarcity, in order to ensure that the regulation up/down capacity is not used for load balancing purposes. However, since the energy scarcity in the real-time model could be interpreted as using a portion of reserved regulation capacity for load balancing, in the ex-post cost analysis a regulation scarcity cost of \$250/MW is used for calculating the energy scarcity cost. The cost coefficients data of day-ahead and real-time models are presented in Table 1 for quick access, where **a** represents the highest energy bids of units.

Table 1: Day-ahead and real-time model cost coefficients

Cost Coefficients	$\mu^{u,R}$	$\mu^{d,R}$	$\mu^{u,B}$	$\mu^{d,B}$	$\mu^{u,G}$	$\mu^{d,G}$	$\mu^{u,F}$	$\mu^{d,F}$	μ^{u,S_e}	μ^{d,S_e}	μ^{u,S_F}	μ^{d,S_F}
Day-ahead Model	0.3**a**	0.3**a**	0.2**a**	0.2**a**								
Real-time Model					1.5**a**	1.2**a**	0.2**a**	0.2**a**	3000	3000	247	152
Ex-Post Cost Calculation					1.5**a**	1.2**a**	0.2**a**	0.2**a**	250	250	247	152

*__a__ represents the highest energy bids of units.

The numerical results of discrete-time (Case 1) and continuous-time (Case 2) models are presented next. The case studies are solved using CPLEX in GAMS environment on a computer with a 4.0GHz i7 processor and 16GB of RAM. The continuous-time look-ahead optimization problem in real-time market is solved for 288 five-minute look-ahead scheduling horizon (covering 24 hours operation). The maximum and minimum computational time of the proposed real-time model in 288 runs is respectively 0.27 and 0.1 seconds.

5.1. Cost Analysis

Day-ahead and real-time operation cost components of the two cases are presented in Table 2. The day-ahead operation cost of Case 2 is greater than Case 1 as the continuous-time model designates more resources to cater for the sub-interval variations of day-ahead net-load. This leads to lower real-time generation adjustment costs for Case 2 compared to Case 1, and zero energy scarcity cost, as shown in Table 2. In addition, the discrete-time model of Case 1 falls short to fully procure the ramp requirement of the

system resulting in a sizable flexible ramp scarcity cost, while the continuous-time model of Case 2 efficiently allocates the ramp resources and leads to zero ramp scarcity cost. The proposed continuous-time model saves $\$39,321.9$ in total day-ahead and real-time operation costs as compared to the discrete-time model, which highlights its economic efficiency.

Table 2: Day-ahead and real-time operation cost components

Model			**Case 1**	**Case 2**
Day-Ahead Operation Cost ($)			**438,922**	**445,031.4**
Real-Time Operation Cost ($)	**Energy cost($)**	**Generation Adjustemnt Up**	14,139.6	10,552
		Generation Adjustemnt Down	5,044.4	2,863
		Energy Scarcity	10,070.3	0
	Flexible Ramp cost($)	**Flexible Ramp Up**	2,987.1	3,016.8
		Flexible Ramp Down	2,567.2	2,826
		Flexible Ramp Scarcity	29,880.6	0
	Total Cost ($)		**64,689.2**	**19,257.9**
Total Operation Cost ($)			**503,611.2**	**464,289.3**

5.2. Real-time Generation Adjustment Schedule

Figs. 6-(a) and (b) present the real-time generation adjustment schedules of generating units for the two cases, which add up to the real-time net-load deviations denoted with purple curves, while the up and down adjustments are respectively presented with positive and negative values and included in same figures. In Figs. 6 the available power capacities of the least expensive resources, e.g., 155MW units, are first deployed to counterbalance the net-load deviation, while more expensive resources, e.g., 197MW and 76MW units, supply the remaining deviation. Note that the nuclear units do not participate in real-time energy and flexible ramp markets.

In Case 2, the continuous-time look-ahead models adequately supply the real-time net-load deviations as denoted in Fig. 6-(b), while in Case 1 the discrete-time look-ahead models fail to properly supply the sub-interval variations of the net-load deviation and lead to energy scarcity events shown with the hatched pattern in Fig. 6-(a). The scarcity events in Fig. 6-(a) coincide with peak net-load hours, where on one hand not adequate resources are committed in day-ahead to accommodate for real-time energy and flexible ramp requirements during these hours, and on the other hand the available flexibility from online resources is not fully leveraged in real-time operation. Further, it is observed in Figs. 6 that during some hours while a set of units

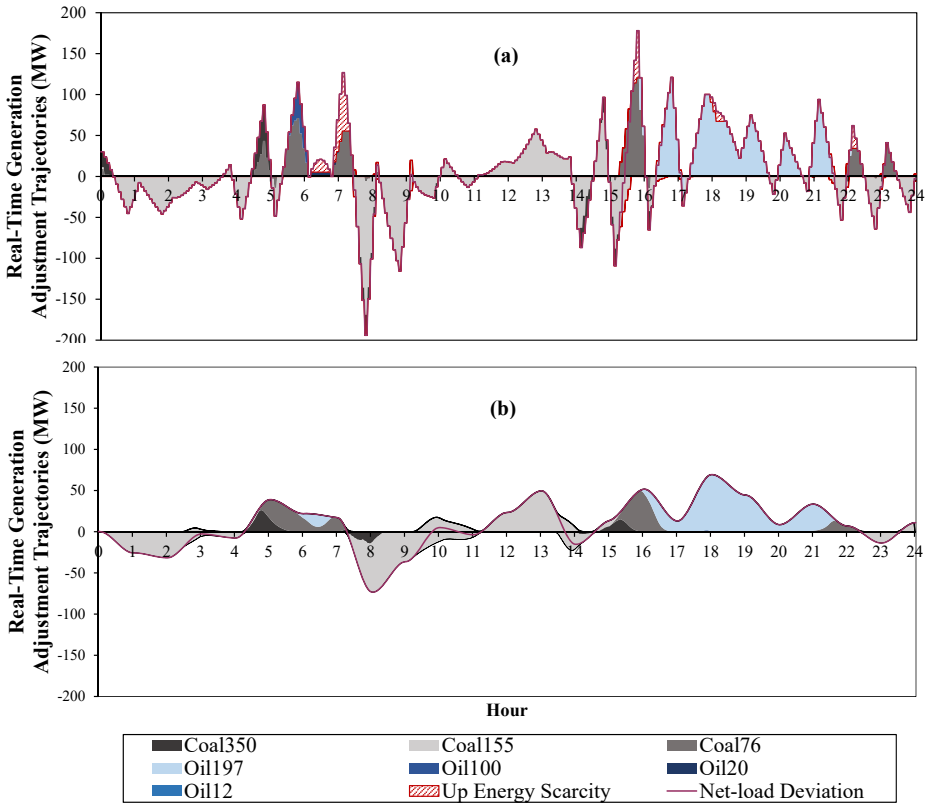

Figure 6: Real-time generation adjustment trajectories in a) Case 1, b) Case 2.

are adjusting their generation upward, another set do the opposite. This indeed tailors the generation schedule of units to enable providing flexible ramp up and down in future times, while supplying the net-load deviation in the present.

5.3. Flexible Ramp Up and Down Schedule

In Figs. 7, the flexible ramp up and down schedules for the two cases are illustrated, where the up and down values are respectively shown in positive and negative for the ease of presentation. As shown in Figs. 7, 155MW units are the main contributors in flexible ramp procurement, due to their fast ramping capability and low flexible ramp cost coefficients, while the 197MW, 76MW, and 350MW units are the next in order. The temporal resolution of up and down flexible ramp requirements in Case 2 is higher than that in Case 1. This shows a more accurate assessment of the power system flexible

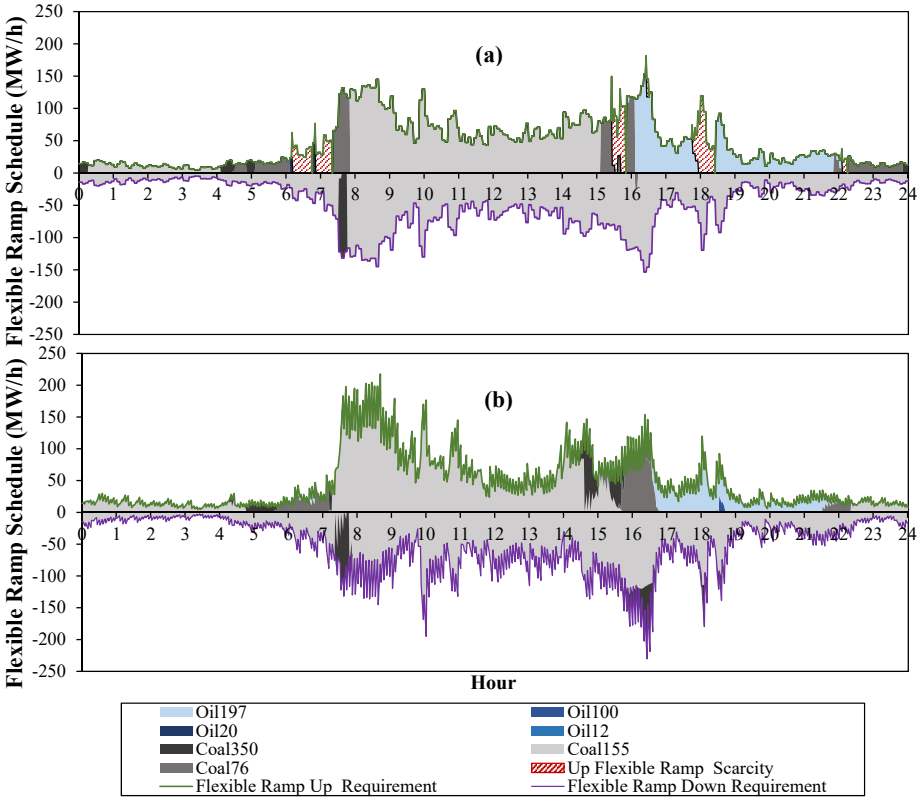

Figure 7: Up and down flexible ramp trajectories in a) Case 1, b) Case 2.

ramp requirements by the continuous-time model in Case 2, and leads to procuring slightly greater flexible ramp compared to Case 1. Though Case 1 is required to reserve less flexible ramp capacity, it still undergoes ramping scarcity events mostly in peak load hours, while Case 2 does not experience any scarcity events attesting to effectiveness of the continuous-time model in scheduling flexible ramp resources.

5.4. Power and Ramping Capacity Allocation

The total committed power and ramping capacity of generating units and their allocation to different services are also shown in Figs. 8 for Case 2. Fig. 8-(a) presents the scheduled day-ahead generation and regulation reserve capacity, as well as the real-time generation adjustments and the power capacity reserved to support providing flexible ramp products. In addition, in Fig. 8-(b) we show the scheduled day-ahead generation ramping,

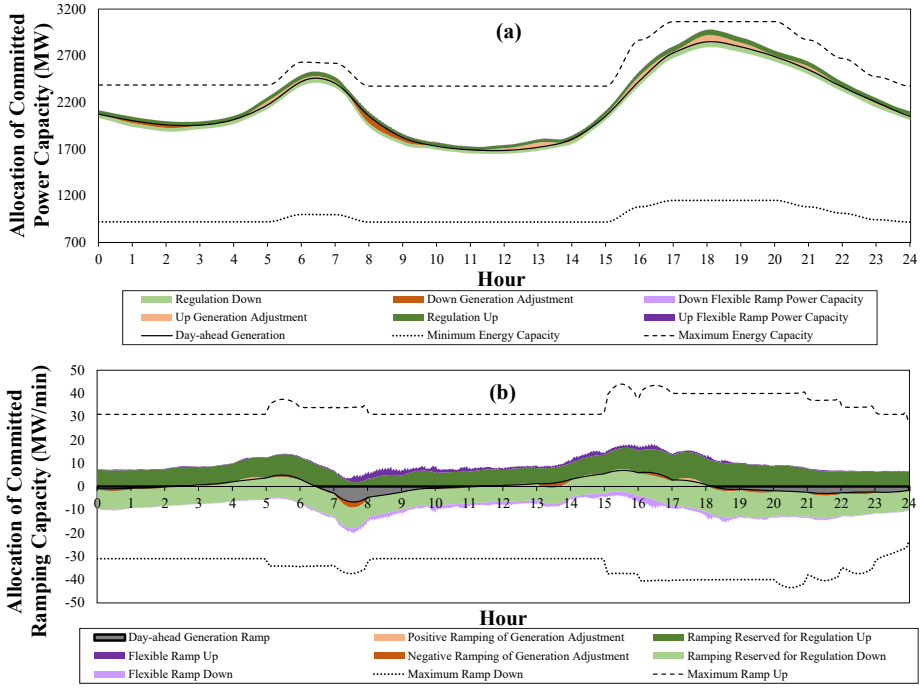

Figure 8: a) Power capacity, and b) ramping capacity allocation of generating units

the reserved regulation ramping, real-time generation adjustment ramping, and the scheduled flexible ramp in real-time. The dashed/dotted lines in Figs. 8 present the aggregated maximum/minimum power and ramp capability of online generating units, in which the impact of continuous-time commitment status trajectories in start-up and shutdown periods is properly embedded. It is shown in Fig. 8 that the furnished envelops provide enough room to secure the procurement of power and ramp requirements and impede scarcity events in real-time operation.

6. Conclusion

This paper presented a continuous-time look-ahead optimization model for co-optimizing the balancing energy and flexible ramp products in real-time power systems operation. In addition, a continuous-time day-ahead operation model was proposed to co-optimize energy, regulation, and balancing reserves in day-ahead operation, for providing adequate energy and ramping capacity for real-time operation. The proposed model utilized ex-

plicit continuous-time trajectories for flexible ramp products, defined as time-derivative of the associated power trajectories. A function space solution method was also proposed to reduce the dimensionality of the continuous-time day-ahead and real-time operation problems, converting them respectively to MILP and LP models of finite dimensions. The simulation results of implementing the proposed continuous-time models on the IEEE-RTS prove their viability in terms of meeting the power system energy and ramp requirements, reducing ramping scarcity events, and their economic efficiency. Future works include considering transmission network limitations, procuring flexible ramp product from energy storage devices, and considering the uncertainty of parameters to develop the stochastic look-ahead scheduling model for real-time market.

Acknowledgement

This work was supported by the United States Department of Energy under grant number DE-OE0000882.

[1] I. E. Agency, Renewables 2017- executive summary (2017).
URL https://www.iea.org/Textbase/npsum/renew2017MRSsum.pdf

[2] Californias renewables portfolio standard (RPS) program, UNION OF CONCERNED SCIENTISTS.
URL https://www.ucsusa.org/sites/default/files/attach/2016/07/california-renewables-portfolio-standard-program.pdf

[3] Reforming the energy vision, New York state Goverment.
URL https://rev.ny.gov/

[4] Y. V. Makarov, C. Loutan, J. Ma, P. De Mello, Operational impacts of wind generation on california power systems, IEEE Trans. on Power Systems 24 (2) (2009) 1039–1050.

[5] H. Ibrahim, M. Ghandour, M. Dimitrova, A. Ilinca, J. Perron, Integration of wind energy into electricity systems: technical challenges and actual solutions, Energy Procedia 6 (2011) 815–824.

[6] CAISO, Flexible ramping product,revised draft final proposal (2015).
URL https://www.caiso.com/Documents/RevisedDraftFinalProposal-FlexibleRampingProduct-2015.pdf

[7] I. G. Marneris, P. N. Biskas, E. A. Bakirtzis, An integrated scheduling approach to underpin flexibility in european power systems, IEEE Trans.on Sustainable Energy 7 (2) (2016) 647–657.

[8] X. Zhang, L. Che, M. Shahidehpour, A. Alabdulwahab, A. Abusorrah, Electricity-natural gas operation planning with hourly demand response for deployment of flexible ramp, IEEE Trans. on Sustainable Energy 7 (3) (2016) 996–1004.

[9] H. Wu, M. Shahidehpour, M. E. Khodayar, Hourly demand response in day-ahead scheduling considering generating unit ramping cost, IEEE Trans. on Power Systems 28 (3) (2013) 2446–2454.

[10] J. Hu, M. R. Sarker, J. Wang, F. Wen, W. Liu, Provision of flexible ramping product by battery energy storage in day-ahead energy and reserve markets, IET Generation, Transmission & Distribution 12 (10) (2018) 2256–2264.

[11] J. Wang, H. Zhong, W. Tang, R. Rajagopal, Q. Xia, C. Kang, Y. Wang, Optimal bidding strategy for microgrids in joint energy and ancillary service markets considering flexible ramping products, Applied Energy 205 (2017) 294–303.

[12] Q. Wang, B.-M. Hodge, Enhancing power system operational flexibility with flexible ramping products: A review, IEEE Trans.on Industrial Informatics 13 (NREL/JA-5D00-67471).

[13] K. H. Abdul-Rahman, H. Alarian, M. Rothleder, P. Ristanovic, B. Vesovic, B. Lu, Enhanced system reliability using flexible ramp constraint in caiso market, in: Power and Energy Society General Meeting, 2012 IEEE, IEEE, 2012, pp. 1–6.

[14] B. Wang, B. F. Hobbs, A flexible ramping product: Can it help real-time dispatch markets approach the stochastic dispatch ideal?, Electric Power Systems Research 109 (2014) 128–140.

[15] B. Wang, B. F. Hobbs, Real-time markets for flexiramp: A stochastic unit commitment-based analysis, IEEE Trans. on Power Systems 31 (2) (2016) 846–860.

[16] B. Zhang, M. Kezunovic, Impact on power system flexibility by electric vehicle participation in ramp market, IEEE Trans. on Smart Grid 7 (3) (2016) 1285–1294.

[17] M. Parvania, A. Scaglione, Generation ramping valuation in day-ahead electricity markets, in: System Sciences (HICSS), 2016 49th Hawaii International Conference on, IEEE, 2016, pp. 2335–2344.

[18] M. Parvania, A. Scaglione, Unit commitment with continuous-time generation and ramping trajectory models, IEEE Transactions on Power Systems 31 (4) (2016) 3169–3178.

[19] M. Parvania, R. Khatami, Continuous-time marginal pricing of electricity, IEEE Transactions on Power Systems 32 (3) (2017) 1960–1969.

[20] G. Angelidis, Day-ahead market enhancements (2018).
URL https://www.caiso.com/Documents/RevisedAppendixC-Day-AheadMarketEnhancementsDraftTechnicalDescription.pdf

[21] N. I. Task, 2.4 report-operating practices, procedures, and tools (2011).

[22] CAISO, Flexible ramping product,revised draft final proposal (2014).
URL https://www.caiso.com/Documents/DraftFinalProposal_FlexibleRampingProduct_includingFMM-EIM.pdf

[23] P. M. Prenter, et al., Splines and variational methods, Courier Corporation, 2008.

[24] R. Khatami, M. Parvania, A. Bagherinezhad, Continuous-time model predictive control for real-time flexibility scheduling of plugin electric vehicles, IFAC-PapersOnLine 51 (28) (2018) 498–503.

[25] A. Bagherinezhad, M. Parvania, Continuous-time flexible ramp scheduling in forward power systems operation, in: Power and Energy Society General Meeting, 2019 IEEE, IEEE, 2019, pp. 1–5.

[26] P. Dierckx, Curve and surface fitting with splines. numeric mathematics and scientific computation, Monographs on numerical analysis. Clarendon Press, Oxford Google Scholar.

[27] I. R. T. Force, The ieee reliability test system-1996, IEEE Trans. Power Systems 14 (3) (1999) 1010–1020.

[28] OASIS, california ISO Operan Access Same-Time Information System, Jan. 2018 (2018).
URL http://oasis.caiso.com

[29] Market optimization, version 49, California ISO (2018).
URL https://bpmcm.caiso.com/BPM%20Document%20Library/Market%20Operations/Appendices_Market%20Operations_V49_redline.pdf